REPORT

Oil in Ice - JIP

Report no.: 24
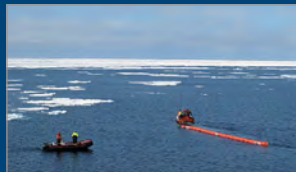
Airborne GPR to Detect Oil Under Snow

John Bradford (CGISS - Boise State University)
David Dickins (DF Dickins Associates)
Per Johan Brandvik (SINTEF Materials & Chemistry)

SINTEF Materials and Chemistry

Marine Environmental Technology

Date: 24.05.2010

www.sintef.no

SINTEF

Preface

SINTEF has in cooperation with SL Ross Environmental Research Ltd and DF Dickins Associates LLC on behalf of the oil companies AGIP KCO, Chevron, ConocoPhillips, Shell, Statoil and Total initiated an extensive R&D program; *Joint industry program on oil spill contingency for Arctic and ice covered waters.* This program was a 3-year program initiated in September 2006 and finalized in December 2009.

The objectives of the program were;
- To improve our ability to protect the Arctic environment against oil spills.
- To provide improved basis for oil spill related decision-making:
- To advance the state-of-the-art in Arctic oil spill response.

The program consisted of the following projects:
- P 1: Fate and Behaviour of Oil Spills in Ice
- P 2: In Situ Burning of Oil Spills in Ice
- P 3: Mechanical Recovery of Oil Spills in Ice
- P 4: Use of Dispersants on Oil Spills in Ice
- P 5: Remote Sensing of Oil Spills in Ice
- P 6: Oil Spill Response Guide
- P 7: Program Administration
- P 8: Field Experiments, Large-Scale Field Experiments in the Barents Sea
- P 9: Oil Distribution and Bioavailability

The program has received additional financial support from the Norwegian Research Council related to technology development (ending December 2010) and financial in kind support from a number of cooperating partners that are presented below. This report presents results from one of the activities under this program.

Stein Erik Sørstrøm
Program Coordinator
(stein.e.sorstrom@sintef.no)

Funding Partners

R&D Partners

Cooperating Partners

BOISE STATE **DICKINS** | **SINTEF**	

Boise State University
Centre for Geophysical
Investigation of the Shallow
Subsurface (CGISS)

Address: 1910 University Drive
                   Boise Idaho USA 83725

Telephone: 208 426 3898

TITLE

Airborne GPR to Detect Oil Under Snow

AUTHORS

John Bradford (CGISS – Boise State University)
David Dickins (DF Dickins Associates) and
Per Johan Brandvik (SINTEF)

CLIENTS

AGIP KCO, Chevron, ConocoPhillips, Shell, Statoil and Total

DATE	PROJECT MANAGER	CHECKED BY
2010-05-24	David Dickins	Peer Review – approved for publication *Geophysics*

ABSTRACT

With recent increased interest in oil and gas exploration and development in the Arctic, comes increased potential for an accidental hydrocarbon release into the cryosphere including within and at the base of snow. There is a critical need to develop effective and reliable methods for detecting such spills. Numerical modeling shows that GPR is sensitive to the presence of oil in the snow pack over a broad range of snow densities and oil types. Oil spills from the surface drain through the snow by the mechanisms of unsaturated flow and form geometrically complex distributions that are controlled by snow stratigraphy. These complex distributions generate an irregular pattern of radar reflections that may be differentiated from natural snow stratigraphy, but in many cases interpretation will not be straightforward. Oil located at base of the snow tends to reduce the impedance contrast with the underlying ice or soil substrate resulting in anomalously low amplitude radar reflections. Results of a controlled field experiment using a helicopter borne, 1000 MHz GPR system, showed that a 2 cm thick oil film trapped between snow and sea ice was detected based on a 51% decrease in reflection strength. This is the first reported test of GPR for the problem of oil detection in and under snow. Our results indicate that GPR has the potential to become a robust tool that can substantially improve oil spill characterization and remediation.

KEY WORDS	ENGLISH	NORWEGIAN
Group 1	Remote Sensing	Fjernmåling
Group 2	Oil Spills in Ice	Olje i is
Selected by Authors	Ground Penetrating Radar	Georadar

ACKNOWLEDGEMENTS

CONTENTS

1   INTRODUCTION AND BACKGROUND

In areas of the Arctic and Antarctic impacted by human activity, there are a variety of scenarios that could result in oil being deposited onto the surface of ice or snow that would necessitate sensing capability beyond visual detection.   For example, in areas of Arctic marine oil exploration or production, a surface blowout may result in a plume of oil droplets falling downwind from a source such as a bottom-founded production structure or an artificial island surrounded by stable or moving ice. Oil deposited in this manner will saturate the existing snow layer and then potentially be covered by fresh snow.   Another potential source of contamination is from surface runoff of oil that has been deposited on the deck of a drilling structure or the surface of an artificial island. At some point, the volume of oil may exceed the containment capacity built into the facility. The spill can then run out onto the ice surface and spread under the snow cover at the snow/ice interface. A photograph of one such spill is shown in Figure 1 which depicts the results of an accidental diesel spill from a ruptured tank barge that was frozen in for the winter in McKinley Bay on the Canadian Beaufort Sea coast during the winter of 1979/80. In this case, oil spreading at the snow/ice interface produced a layer of oil-saturated snow that is clearly visible.

Figure 1   View of oil saturated snow layer on top of the ice following an accidental spill in the
                    Beaufort Sea in 1979. Photo: D. Dickins

A spill resulting from a pipeline leak or rupture also poses a significant risk as illustrated by several recently reported incidents. Christenson (2008) describes two spills near McMurdo Station, Antarctica. In these examples, kerosene-based fuel leaked from a pipeline resulting in spills of 8300 L onto a 0.15 m thick snow cover and 26,500 L onto a 1.27 m thick snow cover. In both cases, the fuel penetrated the snow cover then spread laterally under the snow pack along the snow/sea-ice interface. Determining the extent of fuel migration required digging through the snow to locate contaminated snow and ice. In the Alaskan arctic, a pipeline rupture associated with oil production facilities near Prudhoe Bay in 2005 resulted in the release of approximately 40 $\times 10^4 \, m^3$ of natural gas and 1600 – 4770 L of crude oil (http://www.dec.state.ak.us/spar/perp/response/sum_fy05/050412301 /050412301_index.htm).

The crude oil was released primarily as a fine mist and covered several thousand m^2 of the snow downwind of the spill.

In the spill examples noted above, it is clear that a rapid and effective tool for remote detection and mapping of the oil in and under the snow would have significantly aided remediation efforts. Given the accelerating level of interest in Arctic oil and gas exploration, the need for proven and reliable systems to detect oil trapped in ice and snow environments remains at the forefront of efforts to advance Arctic spill response capabilities. The lack of any reliable and practical operational system to detect and map spilled oil in or under snow continues to be a critical deficiency in Arctic spill response, not only in Alaska but also other rapidly developing areas with similar problems (Sakhalin Island, Russian Barents Sea, North Caspian Sea, Baltic Sea). There is a strong motivation within industry and government agencies to develop a reliable, remote method of detection, which can be carried out economically and safely. Ideally, such a system would have the capability of operating in both airborne and ground-based modes and map the boundaries of contamination over potentially large areas.

In the early 1980's, a substantial research effort was undertaken to analyze and test a variety of technologies to detect oil in or under solid sea ice. These methodologies included radar, electromagnetics and acoustics (Butt et al., 1981; Goodman et al., 1985a; Goodman et al., 1985b; Jones and Kwan, 1982). Results at the time were mixed with lateral variability being one of the primary factors complicating detection of oil within or under ice. While no single technology will likely be effective for oil detection in all conditions, ground-penetrating radar (GPR) has recently emerged as an effective tool for detecting oil under solid ice. As noted by Goodman (2008), there have been major advances in GPR hardware and data processing since 1980. Bradford et al. (2008) describe recent results of laboratory and field experiments that demonstrate successful detection of oil in and under ice with existing commercially available GPR systems.

A number of technologies have proven effective for detecting oil on the surface of snow including infrared photography and laser fluorescence (Fingas and Brown, 2000). Visible light photography may also be effective for detecting oil on the snow surface. These tools will only provide information about the areal extent of the oil and will be ineffective if the oil is not exposed at the snow surface and/or has reached the ambient temperature. Manual probing remains the only proven technology to map the depth distribution of oil within snow. While effective, this approach is labor intensive and time-consuming which ultimately may lead to incomplete location of the spilled oil. GPR has the potential to image both the areal extent and depth distribution of oil in and under snow, but we are not aware of any published studies that have investigated this possibility in detail.

Here we demonstrate that GPR is sensitive to the presence of oil in snow-covered environments and may provide a robust tool for oil spill characterization in snow covered regions. We begin with an analytical discussion followed by numerical models based on observations from published field spills. Finally we describe the results of a controlled field test conducted on the Svalbard archipelago. GPR can be deployed in either surface based, or airborne configurations. Because of safety considerations and/or or the need to cover large areas in a relatively small period of time, we focus on airborne deployment. However, the arguments and analysis tools we discuss are also applicable for surface deployment.

2   BASIC GPR CONCEPTS FOR OIL DETECTION IN SNOW

GPR reflections are generated at boundaries separating materials with differing electromagnetic properties (relative dielectric permittivity, ε, and electric conductivity, σ). In undisturbed, dry snow, electric conductivity is very low ($\sim 10^{-7}$ S/m) and the primary electromagnetic contrasts are related to changes in dielectric permittivity that is largely a function of snow density. As in soils (e.g. Greaves et al., 1996; Huisman et al., 2003), the presence of liquid water can substantially alter the electromagnetic properties of the snow and produce high amplitude reflections. GPR has been used in numerous arctic studies to image stratigraphy and other structures within snow (e.g. Bradford et al., 2009; Harper and Bradford, 2003; Lundberg et al., 2000; Marshall and Koh, 2008; Marshall et al., 2007; Sand and Bruland, 1998), subsurface geology and liquid water below snow and freshwater ice (e.g.Arcone et al., 1992; Arcone et al., 1998; Best et al., 2005; Delaney et al., 1990; Schwamborn et al., 2002), and the sea-ice/sea-water contact (e.g.Bradford et al., 2008; Kovacs, 1977; Kovacs and Morey, 1992; Nyland, 2004).

Detecting oil with GPR that is deposited on to snow or that is trapped at the base of the snowpack is substantially different than detecting oil within or beneath sea ice and requires alternate analysis and experimentation to verify its effectiveness. In particular, the electric conductivity structure of snow differs substantially from that of sea ice. Because electric conductivity controls radar signal attenuation and since snow has very low electric conductivity, the radar signal propagates very effectively through snow. Sea ice has much higher electrical conductivity ($> 10^{-2}$ S/m). The conductivity structure of sea ice varies substantially both laterally and vertically (Morey et al., 1984) and can exhibit a high degree of anisotropy due to preferred crystal alignment (Kovacs and Morey, 1978; Nyland, 2004). Because of its relatively isotropic structure and low conductivity, the problem of oil detection is simpler to formulate for snow than it is for sea ice.

In many cases, a significant relative permittivity contrast exists between snow ($\varepsilon_{sn}\sim 1.4$-2.5) (Langham, 1981), crude oil ($\varepsilon_{oi}\sim 2$-4)(Speight, 2003), and the underlying stratum which may consist of sea ice ($\varepsilon_{si}\sim 4$-7)(Lewis et al., 1994), fresh water ice ($\varepsilon_{fi}\sim 3.16$) (Langham, 1981), or frozen soil ($\varepsilon_{fs}\sim 4$-8) (Daniels, 2007). Note that crude oil also has very low electric conductivity ($\sim 10^{-5}$ S/m). The likely contrasts that exist between these materials suggest that it is possible to image crude oil within snow or at the snow/ice interface using GPR. It is important to recognize that there is overlap in the permittivity range of oil and snow, and oil and sea ice so that in some cases there may not be a contrast at the snow/oil interface when the contaminated layer consists purely of oil. Often, however, the oil contaminated layer will consist of fully or partially oil saturated snow. Because oil has a higher dielectric permittivity than air, replacing air in the pore space with oil will increase the bulk permittivity of the material and produce an anomaly that can potentially be detected using GPR.

2.1 Reflection coefficients for oil within snow

To examine the potential sensitivity of GPR to oil in snow, we begin by computing plane wave reflection coefficients for a wave propagating through the snow and incident on a half-space having the dielectric permittivity of oil. For this and all subsequent examples, we model the dielectric permittivity of snow using the Complex Refractive Index Method (CRIM) (Wharton et al., 1980). As shown by Harper and Bradford (2003), the CRIM equation provides an accurate permittivity-snow density transform in dry snow. Additionally this method enables inclusion of an arbitrary number of other mixture components such as oil and water. In this study, we used the CRIM equation for all snow or snow/oil mixture permittivity calculations. Figure 2A shows reflection coefficients at the snow/oil interface as a function of snow density for a range of oil

dielectric permittivities. Harper and Bradford (2003) showed clear laterally coherent reflections from density contrasts within snow having reflection coefficients of approximately 0.01. Using this observation as a conservative limit, we assume that a reflection coefficient amplitude of 0.01 or greater will produce an identifiable GPR reflection, and find that only at low oil permittivity (ε_{oi}=2) and high snow density (ϱ_{sn}>0.45 g/cm^3, ε_{sn}=1.91) does the reflection coefficient go below this limit. A snow density of greater than 0.45 g/cm^3 is unusual in the cold dry snow pack typical of the Arctic environment. More typically, snow densities will fall in the range of 0.15 g/cm^3 (ε_{sn}=1.27) for fresh snow to 0.35 g/cm^3 (ε_{sn}=1.68) for older windpacked snow (Langham, 1981).
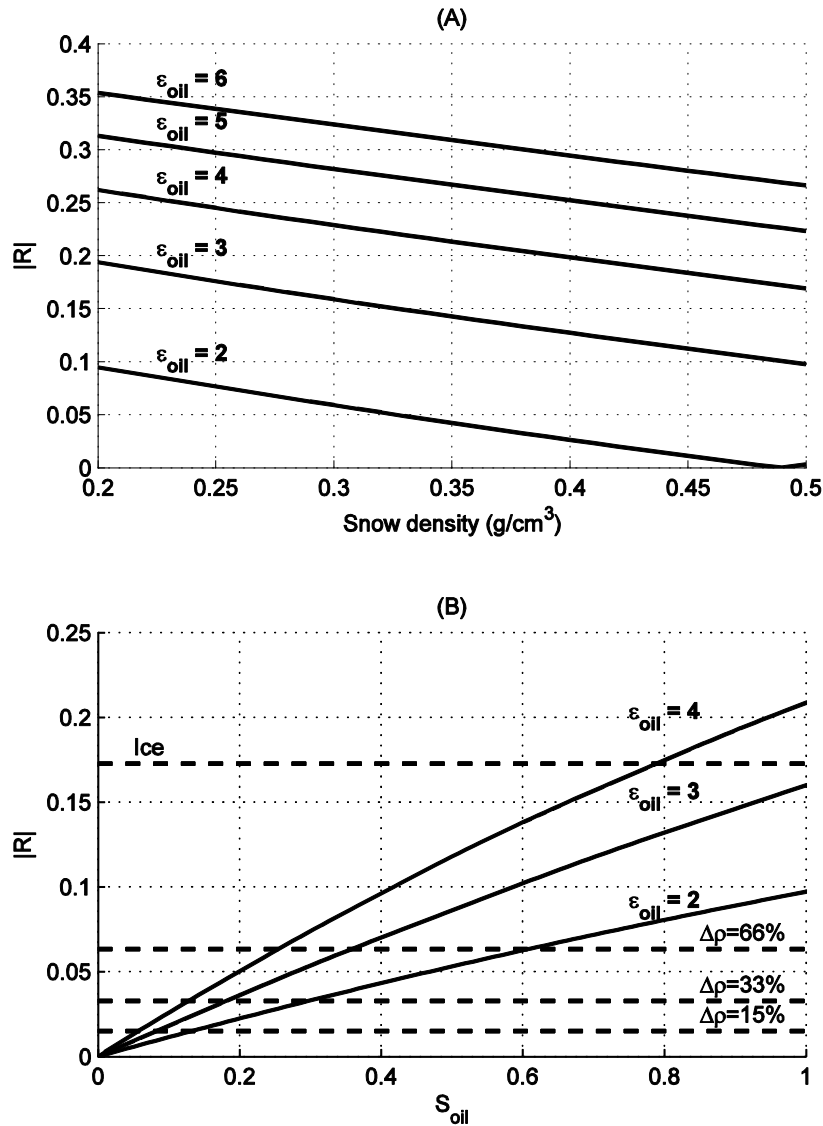
Figure 2 A) Absolute value of plane wave reflection coefficients as a function of snow density and oil dielectric permittivity for a radar signal propagating through snow and incident on a thick layer of oil. B) Absolute value of plane wave reflection coefficients as a function of oil saturation and oil dielectric permittivity at the interface between clean snow (ϱ_s=0.35 g/cm^3) and contaminated snow. Dashed lines show reflection coefficients from clean snow layers with differing density that might be present in the undisturbed snow. These results show that oil present within or beneath snow will produce measurable GPR reflections over a broad range of snow densities, oil saturations, and oil dielectric permittivities.

In our second example, we compute reflection coefficients with a snow density of 0.35 g/cm^3 and a lower half space consisting of snow with partial oil saturation, S_{oi} (Figure 2B). We vary both the saturation and oil dielectric permittivity. Reflection coefficient amplitudes vary from 0 to over 0.2 depending on saturation and oil permittivity. For ε_{oi}=2, the |R|=0.01 threshold is reached for for S_{oi}>0.09 and at ε_{oi}=4 the threshold is reached at S_{oi}>0.04.

Snow is a stratified medium and reflections are generated where density variations are present between snow layers. In a mature snowpack, where some melting has occurred or if there has been a rain on snow event, ice layers may be present and will produce GPR reflections. By plotting reflection coefficients for uncontaminated snow with density contrasts of 15%, 33%, and 66% relative to the background snow density of 0.35 g/cm^3, we find that reflection coefficient amplitudes range from 0.015 - 0.063 (Figure 2B). A reflection from a fresh water ice layer within the snow will produce a high amplitude reflection (|R|=0.17), which approaches the highest amplitudes we might expect from fully oil saturated snow.

In summary, oil within snow may generate reflections that have amplitudes in the same range as those for contrasts that may occur naturally. This non-uniqueness limits our interpretation to identifying anomalies and reflector geometries that are consistent with oilflow processes and differentiated from natural background snow stratigraphy. Positive identification of oil will require snow sampling following anomaly detection and interpretation.

2.2 Oil at the base of the snowpack

2.2.1 Oil spreading behavior on ice

The spreading of oil on an ice surface is similar to spreading of oil on land or frozen soil. The density and viscosity of the oil controls the rate of spreading. Oil spilled on ice spreads much more slowly than on water and covers a smaller final area with much thicker equilibrium thickness than on water. On smooth ice, surface tension limits the minimum thickness of oil to a range from a few mm to cm. However, as oil pools in topographic lows, the final contaminated area is dictated largely by the surface roughness of the ice. Figure 3 shows the estimated spill area on ice as a function of spill size and ice roughness and is drawn from some of the earliest experimental spill results documented by McMinn (1972).
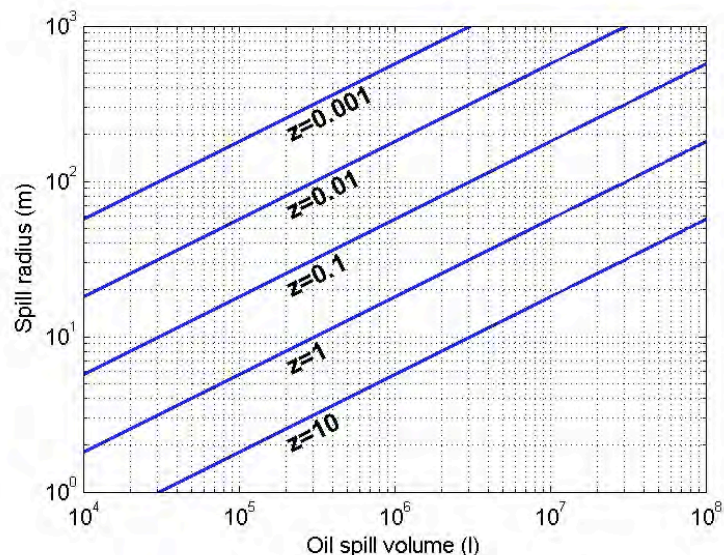
Figure 3 Oil spreading on the surface of ice (McMinn, 1972). z is the effective roughness height in meters.

It is clear that ice roughness impacts spill area significantly. Smooth first-year sea ice has an average surface roughness in the 3 – 30 cm range, with roughness defined simply as the mean peak-to-trough height. Individual ice deformation features such as rafting, rubble and pressure ridges can lead to localized increases in roughness up to tens of meters in elevation above sea level (for example, in the case of extreme grounded ridges along the seaward edge of the fast ice). Any oil spilled on the surface of rough ice may be completely contained in thick pools bounded by ridge sails and ice blocks.

Figure 2B shows that the presence of oil in the pore space brings the snow/contaminated snow reflection coefficient closer to the snow/ice reflection coefficient. This indicates that for all but perhaps the highest permittivity oils at high saturations, the presence of oil at the base of the snow effectively decrease the permittivity contrast between the snow and underlying ice or frozen soil. In a typical scenario an anomalous decrease in reflection amplitude should be observed where oil is present and the reflection amplitude alone may be a valuable diagnostic. Up to this point we have only discussed the case of a thick contaminated layer, with "thick" being defined as something much larger than the GPR wavelength. However, oil may be present at the base or within the snow in layers that are substantially thinner than the wavelength of the signal. Understanding the thin layer response is critical for oil identification.

2.2.2   Thin layer reflection analysis

The resolving power of the GPR system limits the thickness of oil that can be measured directly; that is by measuring the travel time difference between wavelets reflected from the top and bottom of a layer. The wavelength of the signal controls the resolution, with a shorter wavelength signal capable of resolving finer features. When a layer is thinner than about ¼ of the dominate wavelength of the GPR signal, it is impossible to clearly differentiate wavelets reflected from the top and bottom of the layer (Widess, 1973). Consequently a simple reflector map is not sufficient to confidently infer the presence of oil under or within snow. In a typical scenario, an oil film trapped at the snow/ice interface will be on the order of less than 5 cm which will be below the ¼ wavelength resolution of most commercial radar systems which have an upper frequency limit of 1-1.5 GHz and corresponding wavelength in snow on the order of 15-30 cm. In this case, rather than relying on a direct measure of traveltime differences, we utilize instantaneous attributes including the instantaneous phase, instantaneous frequency (derivative of the phase) and instantaneous amplitude (also referred to as the reflection strength). Attribute analysis is commonly used in oil and gas exploration to identify reservoirs of hydrocarbon in sedimentary rocks using seismic reflection data (Chopra and Marfurt, 2005). Here we extend their use to detecting oil layers at the base of the snow with GPR reflections.

Instantaneous attribute measurements can be made from typical fixed antenna GPR data which are relatively fast and inexpensive to acquire. A number of studies have shown that attribute analysis of GPR data can be effective for identifying contaminants in sedimentary groundwater systems (Bradford, 2007; Bradford and Deeds, 2006; Bradford and Wu, 2007; Orlando, 2002). Similar methods for detecting oil spills under sea ice were first proposed by Goodman et al. (1985b), and Bradford et al. (2008) used instantaneous attributes to image oil under sea ice in laboratory and field experiments. It is important to recognize that buried oil will not produce a unique GPR attribute but will only provide an indication of an electric permittivity or conductivity anomaly. Correctly interpreting oil induced anomalies requires comparison to the background or oil-free GPR response, and ultimately positive verification requires direct sampling.

2.2.3   Modeling the thin layer GPR response

To begin to understand the GPR response to thin layers of oil at the snow/ice interface we first assume that the lateral dimensions of the spill and the scale of variability are large relative to the wavelength of the GPR signal. Further, we assume smooth lateral variations in the snow pack and sea ice. These assumptions allow us to utilize the reflectivity method which is a 1D plane-wave solution to the electromagnetic wave equation and is analogous to reflectivity models utilized in seismology to simulate horizontal shear waves. We utilize the well known recursion formula given by Müller (1985) for horizontally polarized transverse waves to compute the reflected wave field for a plane wave at normal incidence on a stack of laterally homogeneous layers with arbitrary layer thicknesses and permittivity contrasts. Our formulation utilizes the full complex electromagnetic wavenumber and thereby is capable of modeling wave propagation through lossy, conductive media. We used a 1200 MHz Ricker wavelet for the source.   Note that Løseth and Ursin (2007) discuss a general implementation of the reflectivity method for electromagnetic fields.

We simulated the GPR response to a thin layer of oil present at the interface between snow and sea ice for a range of oil and snow thickness combinations as depicted in Figure 4A. For this example, we consider a snow density of 0.26 g/cm^3 (ε_{sn} = 1.5), oil permittivy of ε_{oi} = 2.2 and assume that the electric conductivity of the snow and oil are negligible. We use a sea ice permittivity of ε_{si} = 5.0 and conductivity of σ_{si}=0.02 S/m. The oil permittivity is at the low end of the range for oils. Replacing air in the pore space with this low permittivity oil produces a minimal change in the bulk snow properties. Therefore we expect that the anomalous GPR response will be minimal relative to what would be observed with higher permittivity oils. We varied the oil film thickness from 0 – 5 cm while holding the snow cover constant at 20 cm. We then decreased the snow cover from 20 – 0 cm while holding the oil film constant at 5 cm thick.

In the synthetic GPR data, the most prominent reflection originates from the top of the ice (Figure 4B) and is therefore the easiest to identify. Although the oil film is less than the ¼ wavelength vertical resolution criterion, the top of ice reflection attributes are strongly dependent on the presence of the oil film and its thickness. Figure 4B shows qualitatively a decrease in amplitude which is evident from models 40 - 200. We find that the reflection strength decreases by 45% as the oil thickness increases from 0 – 5 cm (Figure 4C). For an oil film of only 1.3 cm thick, there is a 15% drop in reflection strength.

To determine if a 15% change in reflection amplitude can likely be detected in field data, consider GPR data we acquired in 2006 along a fjord in Svalbard, Norway.   We utilized a Sensors and Software PulseEKKO Pro GPR system with 1000 MHz antennas mounted beneath a helicopter flying at an altitude of 20 m and a speed of 7.71 – 10.28 m/s to acquire a 600 m long profile of the snow/sea ice contact. The snow thickness varied from 15- 50 cm. The standard deviation of the snow/ice reflection amplitude was ±11% of the mean. This variability includes both background and system noise as well as natural variability due to snow thickness, surface roughness, and electric property heterogeneity. It should therefore be possible to detect anomalies greater than 11% of the mean reflection amplitude. Assuming that the Svalbard profile is characteristic of the short wavelength heterogeneity in snow and ice, we conclude that in many cases it should be possible to detect the low-amplitude reflection anomaly induced by the presence oil films of 1 cm thick or greater when using with pulsed radar operating above 1000 MHz.

The reflection strength is largely independent of the snow thickness because the reflection from the top of the snow is relatively low amplitude and results only in weak interference with the snow/ice reflection. However, significant frequency and phase anomalies are present where both the oil and snow layers pinch out (Figures 4D and 4E).

However, these attributes tend to be highly sensitive to background noise in the data and because of this complication we believe the reflection strength will be the most robust indicator of oil in the field.
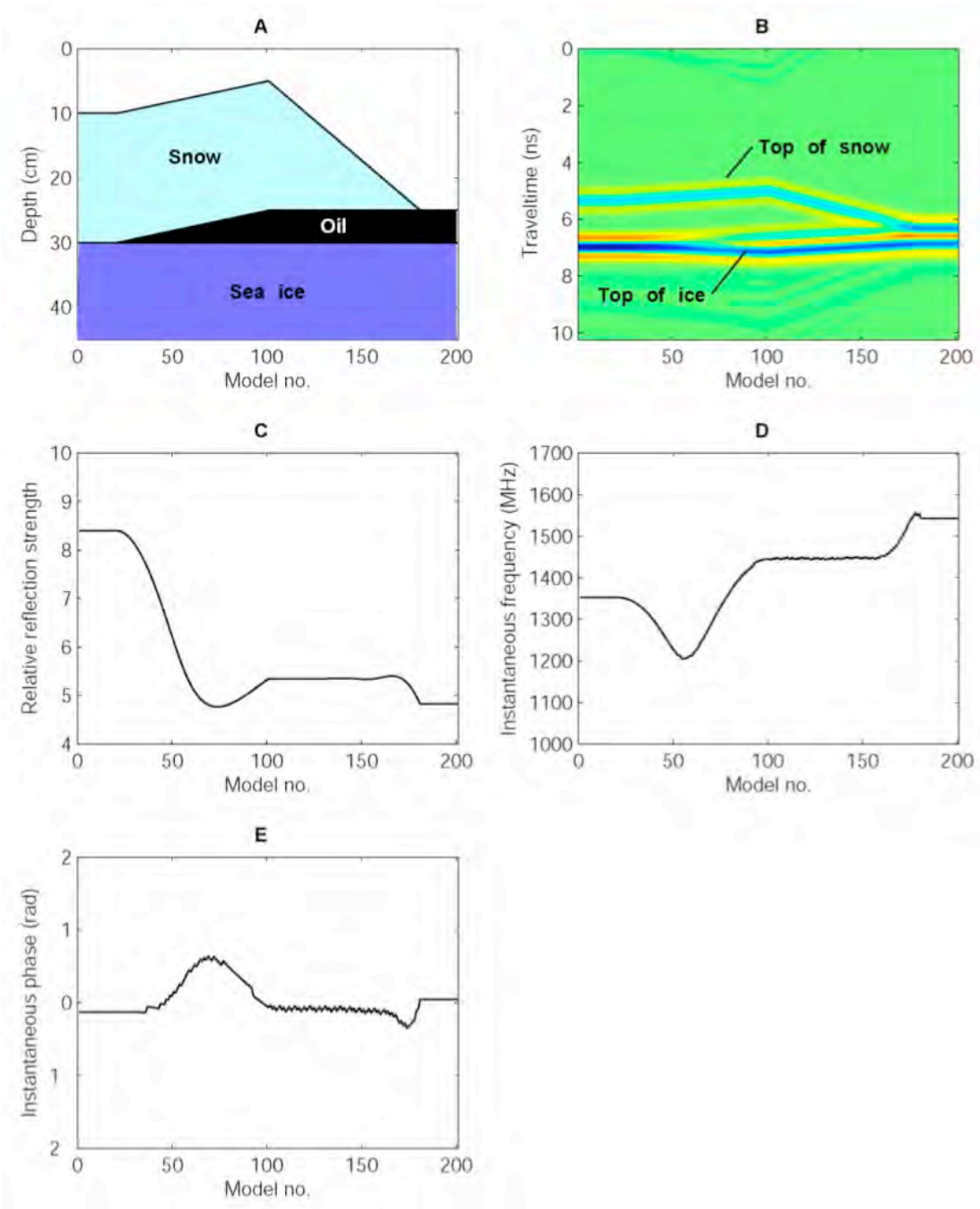
Figure 4. A) Set of 1D models simulating a range of possible spill conditions. B)Synthetic GPR traces generated using the models shown in A). C), D), and E) Relative reflection strength, instantaneous frequency, and instantaneous phase for the top of ice reflection. Although the oil film is not well resolved, the top of ice reflection attributes are strongly dependent on the presence of the oil film and its thickness. The reflection strength is largely independent of the snow thickness in this case. However, significant frequency and phase anomalies are present where the oil and snow layers pinch out.

3 NUMERICAL AND PHYSICAL MODELS OF FIELD SPILLS

Given the relatively simple models described above, our objective now is to evaluate the radar response to a variety of spill scenarios and to include many of the complications that occur under field conditions. Regulatory procedures and remoteness make conducting controlled field spills in the Arctic expensive and logistically difficult so with the exception of one example, we are relying primarily on numerical simulations based on documented spills. We consider three scenarios: 1) oil spilled on top of snow which drains through the snow pack using data from controlled field studies conducted by Mackay (1974), 2) oil spreading along a snow/frozen-ground interface utilizing data from a recent spill on the North Slope of Alaska (http://www.dec.state.ak.us/spar/perp/response/sum_fy06/060302301/060302301_index.htm), and 3) a controlled field spill we conducted on Van Mijenfjord near the SINTEF field research facility near Sveagruva, Svalbard to simulate oil spilled on bare sea-ice that is subsequently covered by snow.

3.1 Oil spill on snow

The spreading characteristics of oil on snow have been studied since the early 1970's (Mackay, 1974; Mackay et al., 1975). As noted by Owens et al. (2005) the distribution of oil after a spill onto the snow surface depends strongly on snow conditions. The snow in most cases will act as a porous medium and the oil will drain through the snow, but in some cases may remain pooled at the surface. Once in the snow, the oil distribution is complex and is influenced by changes in snow permeability that lead to zones of lateral spreading connected by vertical migration channels. Changes in permeability can be caused by mechanisms ranging from small changes in snow grain packing to large changes such as the presence of ice layers. Owens et al. (2005) point out that these complications make it difficult for responders to predict where the oil might be located and therefore slows the cleanup process.

To test the ability of GPR to detect a realistic distribution of oil resulting from a spill onto the snow surface, we constructed a model based on one of a series of carefully controlled and documented spills (Mackay, 1974; Mackay et al., 1975). For the experimental data we utilize, they spilled 0.63 m^3 of cold (0°C) oil on to the surface of a 50 – 60 cm thick snowpack. After 30 hrs, they excavated a trench through the spill and mapped the distribution of oil along the trench wall. Oil was found to have reached the base of the snow in some locations with vertical migration interrupted by zones of lateral spreading along thin ice layers that were present in the snowpack. It is not unusual to find ice layers in snow that has no liquid water present and is well below freezing. Water may be present early in the season either through melting during a warm period or from a rain on snow event. This water infiltrates the snowpack and refreezes.

3.1.1 Model generation.

We digitized Mackay's (1974) oil distribution cross-section to produce a binary map indicating either the presence or lack of oil. We then constructed an electric property model assuming a snow density of 0.35 g/cm^3 and oil saturation of 50% in all oiled areas. We inserted 0.5 cm thick ice layers where noted in Mackay's (1974) oil distribution map. We used a representative sea ice permittivity (ε_{si}=5) for the base of the model, however this is largely aesthetic as the oil does not reach the base of snow in this cross section and the bottom reflection is used primarily as a marker. The dielectric permittivities of the snow and oil are given in Table 1 and the resulting electromagnetic velocity model is shown in Figure 5A following.

The oiled area appears as a low velocity zone between 1 and 2 m distance. Note the two ice layers sloping from left to right across the model with distinct zones of oil spreading laterally along the ice layers. Distinct vertical migration channels are clearly evident as well.

Table 1. Relative dielectric permittivities used for the oil spill on snow and oil spreading at the snow/frozen ground interface simulations. Electric conductivity was assumed negligible for all materials.

Material	ε
Snow	1.68
Oil	2.2
Fresh water ice	3.16
Frozen soil	3.5
Sea ice	5.0

To simulate the radar response we utilized a 4th order time/4th order space, finite difference time-domain (FDTD) simulation that solves the 2D scalar wave equation as described by Levander (1989). Note that Maxwell's equations reduce to the scalar wave equation for 2D isotropic media with the electric field polarized perpendicular to the model plane. We accomplish efficient simulation of long radar profiles using the exploding reflector implementation available with ProMAX™ processing software with sources and receivers located 1 m above the snow surface.

This approach simulates acquisition of a full profile of closely spaced radar traces with common transmitter/receiver positions and eliminates the need to simulate individual source points. By placing the sources above the snow surface, we model the effect of scattering at the air/snow interface that would be observed for airborne deployment. This exploding reflector model does not account for radiation patterns. However, the radiation pattern is radially uniform for a dipole that is polarized perpendicular to the image plane and radiating in a homogenous medium. This is a reasonable approximation in the case where antenna is suspended in air above the surface. Additionally, the model does not account for source receiver separation. The source and recording datum in all of our models is a minimum of 5 times the nominal 20 cm separation of a typical 1 GHZ antenna so that the zero-offset approximation is reasonable. The source wavelet is the first derivative of a Guassian with a dominant frequency of 1000 MHz. Trace spacing for processing and display is 0.85 cm. We added 5% random noise relative to the maximum amplitude reflected arrival (Figure 5B). The result is a background noise level that is higher than what we typically observe in field data acquired with our commercial GPR system.
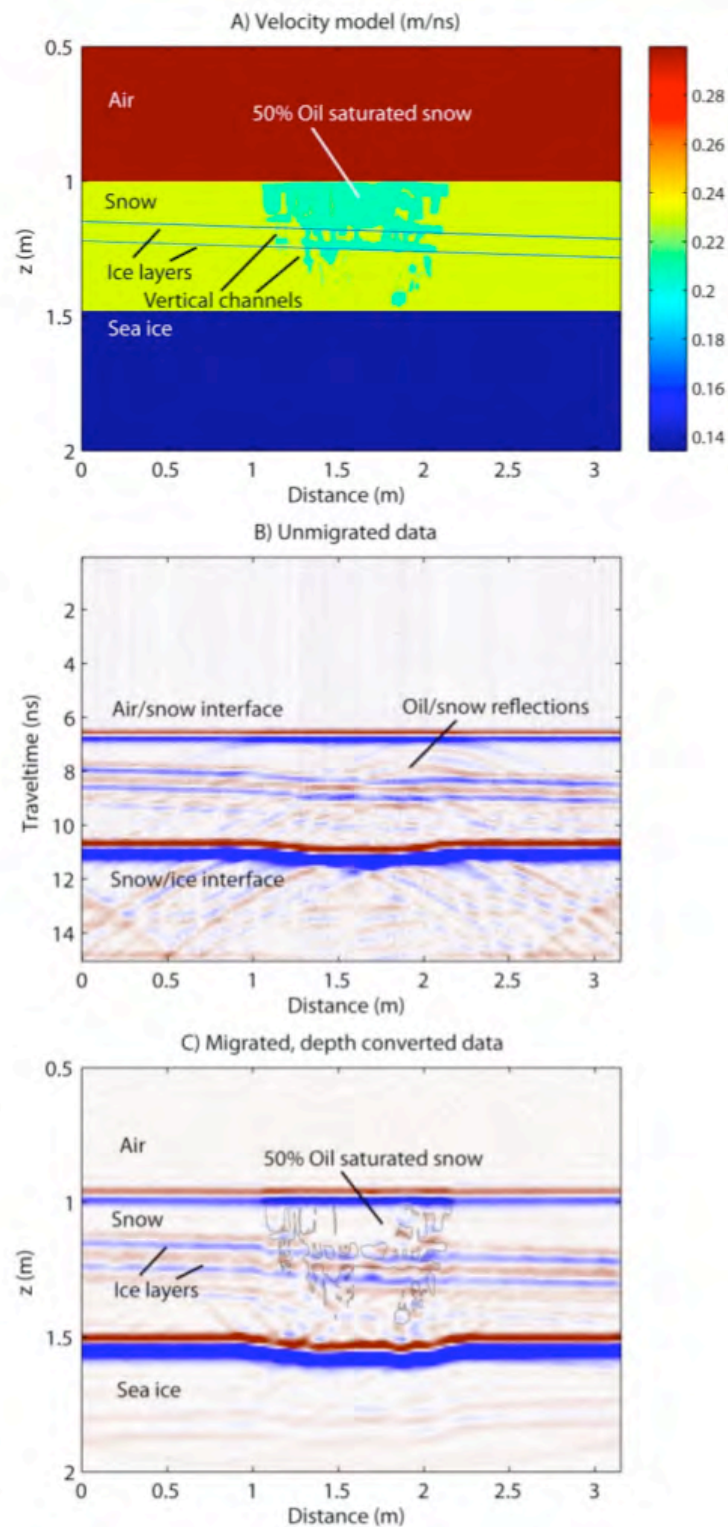
Figure 5. A) The electromagnetic velocity model digitized from the cross section mapped by Mackay et al. (1974) after a spill of cold oil on the top of the snow pack. B) Model GPR data show a complex pattern of scattering caused by the irregular oil distibution. C) Overlaying the outline of the oil distribution onto the phase-shift migrated, depth converted section reveals a detailed image of the oil boundaries. Reflection amplitudes from the oil contaminated snow are substantially lower than those from the ice layers.

3.1.2 Results

The air/snow reflection and snow/sea-ice reflection are clearly evident as high amplitude arrivals at just over 6 ns and 10 ns respectively. The two ice layers produce high-amplitude left-to-right dipping reflections that interfere but are resolved (i.e., the wavelet centroids are well separated). The zone of oiled snow creates a complex pattern of scattered energy that is evident as low amplitude diffractions between distances of 1 - 2 m and arrival times from 6 -10 ns. Reflections from the contaminated snow boundaries interfere with the ice layer reflections causing amplitude variations along these horizons. Additionally, the contaminated snow is a low velocity zone (Figure 5A) and a velocity push down is observed along the snow/sea-ice reflection below the oil. The reflection amplitude from the air/snow interface is 47% higher over the contaminated interval and well above the noise level in the data.

We applied phase-shift migration to the data with a 1D velocity model using the velocities of the air and snow (Table 1, Figure 5C). We then depth converted the data and overlaid an outline of the oil distribution. This simple migration produces a detailed image of the reflections from the oil boundaries, but because it utilizes a 1D velocity model, some migration artifacts are produced due to the lateral velocity contrasts and velocity push down is not corrected. Nevertheless, this is a migration that could easily be implemented for rapid field assessment and clarifies the image for interpretation.

3.2 Oil spreading along a snow/frozen ground interface

In this example, we simulate the GPR response to a spill that occurred on Alaska's North Slope in early March of 2006 (http://www.dec.state.ak.us/spar/perp/response/sum_fy06/060302301/060302301_index.htm). A 0.64 cm diameter hole developed in a transit oil line and began spilling oil beneath ~1.5 m of snow overlying frozen tundra adjacent to the pipeline. The spill went undetected for 3-5 days resulting in an estimated 760000 L of crude oil being released to the environment. This is the largest spill that has occurred on the North Slope in over 30 years of oil exploration and production. In this case, the spill had not reached ambient temperatures by the time remediation efforts began and airborne infrared photography provided an image of the areal extent of the spill. However, mapping the spill thickness for volume estimation and remediation design required manual probing from the surface of the snow, a time-consuming and potentially dangerous operation.

The land surface adjacent to the pipeline is characterized by the regular distribution of troughs and highs that are characteristic of patterned ground which forms due to freeze thaw processes in Arctic regions (Ritter et al., 2002). As the oil flowed along the ground surface it filled in the topographic lows producing pools up to 28 cm thick.   The Alaska Department of Environmental Conservation (ADEC) has made a limited amount of spill characterization data available which we utilized to construct an electrical property model of the spill.

3.2.1 Model construction

We based our model on an oil thickness map which was contoured from manual probe data acquired on a 3 x 3 m grid.   We constructed a cross section that passes through the spill where oil reaches its greatest thickness (Figure 6A). No snow physical property data are available so we assumed a snow density of 0.35 g/cm^3. While this is likely a higher density than the dry cold snow that was present at the time of the spill, it tends to decrease the contrast between oil and snow and thereby produces the minimal, end-member response in our model. We assume that the oil fully saturated the snow as it flowed out laterally and reached a level equilibrium upper surface.

To simulate wicking of the oil into the snow above the saturated zone, we smoothed the oiled/clean snow boundary over a 5 cm vertical interval. We assume dielectric permittivities of ε_{fs}=3.5 for the frozen soil, and ε_{oi}=2.2 for the crude oil. To simulate short wavelength variability in surface topography due to vegetation, we superimposed random $\pm$ 10 cm vertical variations, smoothed laterally over 15 cm, on to the long wavelength patterned ground topography. We placed a mirror image of the snow and soil model with no oil contamination on the left hand side of the model to compare the contaminated response to the background response. The dielectric permittivities of the snow, oil and frozen soil are given in Table 1 and the resulting velocity model is shown in Figure 6A.

To simulate the GPR data, we used the FDTD exploding reflector model described in the previous section. Since in this case the oil was present in relatively thick pools, we relaxed our resolution requirements and used a lower frequency, 500 MHz source pulse. Again we placed the sources and receivers 1 m above the snow surface. For processing and display the data were resampled to a trace spacing of 1.5 cm. After the data were generated, we added random noise to the traces with a 20:1 ratio of noise to maximum reflection amplitude as in the previous example.
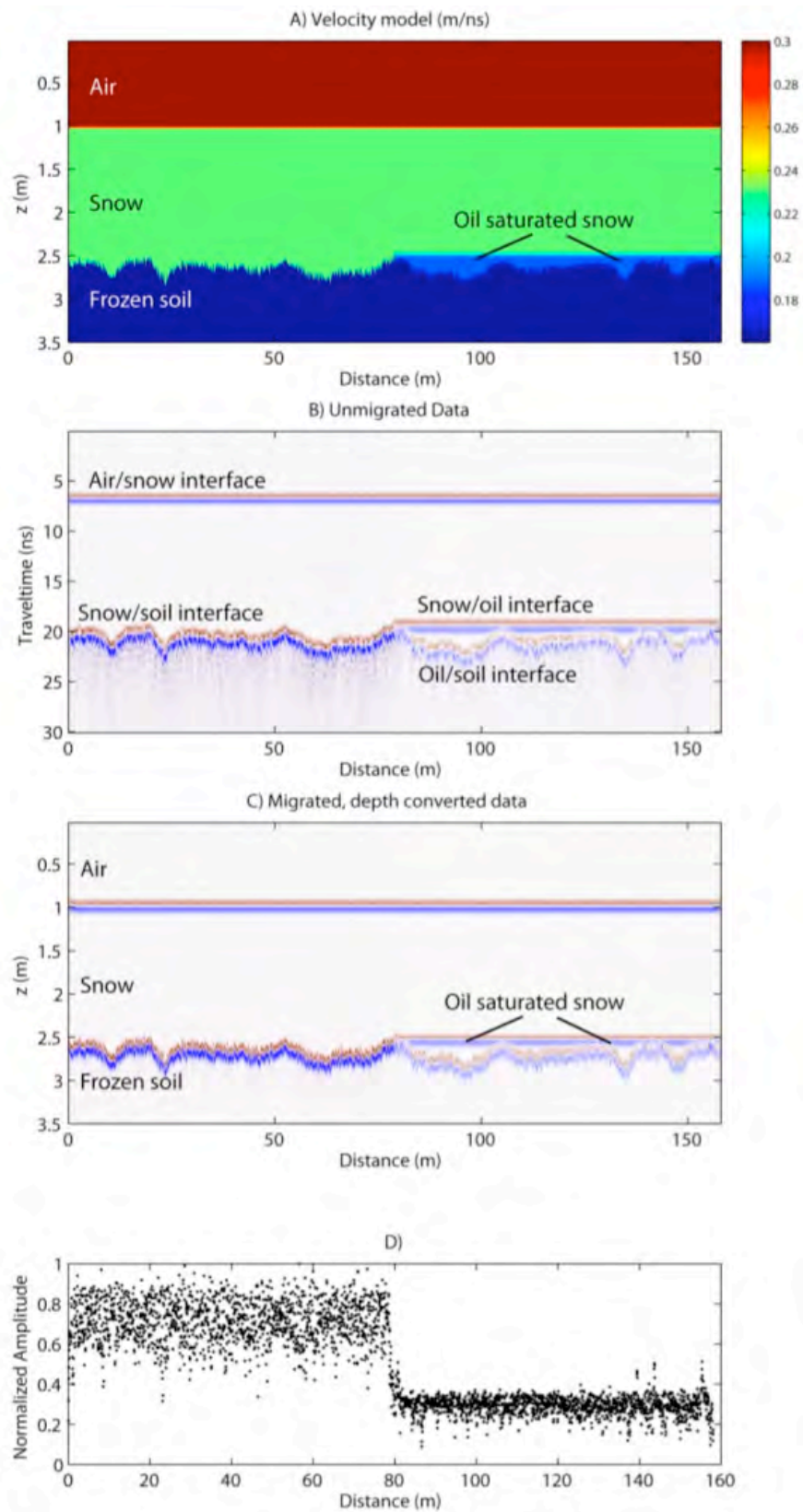
Figure 6. Simulation of the North Slope pipeline spill. A) Velocity model derived from a cross section throught the measured oil thickness contour map, B) modeled GPR data, C) data in B after phase-shift migration and depth conversion, D) amplitude of the snow/soil interface reflection taken from C. The decrease in amplitude occurs because oil in the pore space decreases the permittivity contrast at the snow/soil interface.

3.2.2 Results

The reflection from the clean snow/oil-saturated snow boundary is clearly visible as a horizontal horizon at 18 ns between distances of 80 to 160 m (Figure 6B). The oil is present in relatively thick pools with an average thickness of 12.6 cm. This thickness is greater than ¼ of the 40.4 cm GPR wavelength in the oil at 500 MHz and the oil saturated layer is vertically resolved along most of the profile. The soil reflection is complex and numerous diffractions are generated from the short wavelength heterogeneity present along the surface. Phase-shift migration improves the lateral resolution of the soil interface (Figure 6C) but does not substantially improve interpretability of the profile. The most striking feature of the profile is the drop in soil interface reflection amplitude by a factor of more than 2 at the transition from clean to oil saturated snow at a distance of 80 m (Figure 6D). Oil in the pore space increases the bulk permittivity of the snow and decreases the contrast between the snow and frozen soil. This decrease is well above the noise level which includes amplitude variations caused by focusing and defocusing along the irregular interface as well as random noise.

3.3 Controlled field test: thin film of oil at the snow/ice interface

As a final test we constructed a physical model by conducting a controlled field spill near the SINTEF field facility near Sveagruva, Svalbard. Our primary objective was to evaluate the use of GPR deployed from a helicopter to detect a crude oil spill on sea ice that is buried by snow.

3.3.1 Test cell construction.

The experiment site was prepared by constructing two ~4.5 m x 4.5 m test cells on the ice surface; the cells were constructed by clearing the snow, then scraping and smoothing the ice surface to promote uniform spreading of the oil. The snow surrounding the cell was a dense windpack and provided adequate containment of the oil. One cell served as the experiment control with no oil. In the oiled cell, 400 L of Stratfjord crude were first warmed to room temperature in an indoor facility then poured onto the ice surface. (Figure 6). The oil flowed smoothly and formed a relatively uniform layer. Following the GPR surveys, we measured the oil thickness using a syringe sampling tube every 30 cm. Samples were collected along two perpendicular sides of the containment cell and located 60 cm from the outer boundary. The average oil thickness was 2 cm ± 1 cm. Approximately 1.5 m^2 area remained free of oil in one corner of the cell because of minor variation in ice topography.

Figure 7. Photograph of Sintef personnel pouring oil into the spill containment area for the oil under snow field experiment.

Air temperature during the spill and data acquisition reached a high of less than -13C. At these temperatures, the oil rapidly became highly viscous and immobile, preventing further migration outside of the test cell. To prevent accidental contact of wildlife with the oil, a trip wire system with flares was installed around the perimeter of the spill. Following the spill, high winds resulted in natural windblown snow cover, 5 – 10 cm thick over the spill and 5 – 20 cm thick over the control cell. This natural snow cover was deemed preferable to artificially covering the spill with shoveled snow as it produced a more realistic spill simulation. While the snow thickness was variable and differed over the control and test cells, we could not have leveled the snow cover without substantially disturbing the snow; this would have been detrimental to the experiment. Since the oil was highly viscous, there was very little mixing of the snow cover and oil and we observed a distinct boundary between the oil and snow when measuring oil thickness.

3.3.2   Data acquisition.

Data were acquired with a Sensors and Software PulseEKKO Pro using 1000 MHz shielded antennas in bistatic mode with 17 cm separation between the source and receiver. When deployed in air, this system generates a pulsed waveform with a 500 – 2600 MHz bandwidth and a dominant frequency of 1300 MHz. The radar system was suspended from the helicopter's cargo hook mount (Figure 8) and flown across the test cells (Figure 9) at altitudes of 5, 10, 15, and 20 m and speeds of 2.57, 5.14, 7.71, and 10.28 m/s.

Figure 8. Photograph showing the 1000 MHz shielded antennas suspended from the cargo hook of the helicopter.
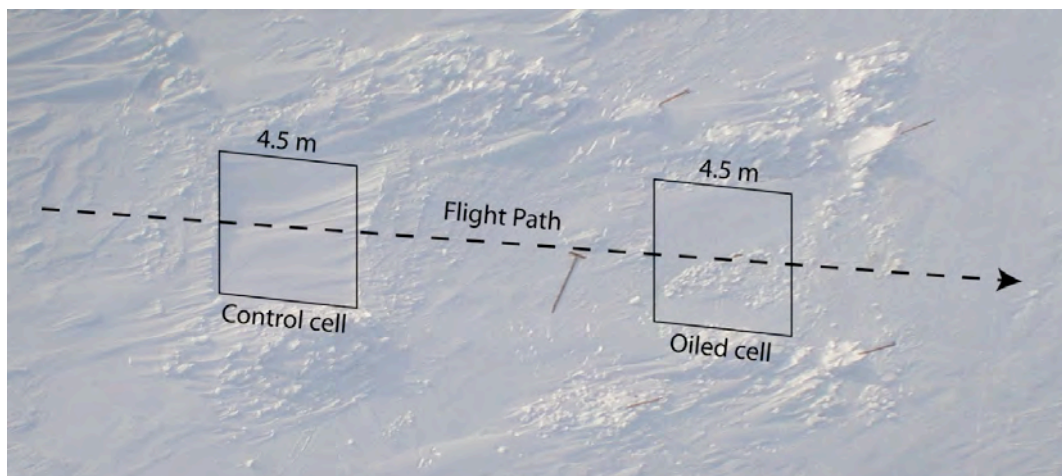

Figure 9. Overhead photograph of the snow covered test cells and helicopter flight path.

Prior to data analysis, the dielectric permittivity of the crude oil was measured by placing a 20 cm thick layer of oil in a plastic container then acquiring radar traces with the antennas suspended above the oil. We then measured the traveltime difference between the reflection from the top of the oil and the reflection from the base of the oil. Dividing twice the oil thickness by the two way traveltime yields the velocity which is then converted to relative electric permittivity according to

$$\varepsilon = \left(\frac{c}{v}\right)^2$$, where c is the speed of light and v is the measured velocity. This procedure yielded a

value of ε_{oi} = 3.5. For the windblown snowcover, we measured the snow depth (18 cm) in the center of the test cell after GPR data acquisition, then measured the traveltime difference (Δt = 1.4 ns) between the air/snow and snow/ice reflections at the same location, giving ε_{sn} = 1.4. We obtained a representative dielectric permittivity for the undisturbed snow cover surrounding the pits using a snow depth measurement (27 cm) located halfway between the two pits. At this location the two way travel time (Δt = 2.8 ns) yields an estimated permittivity of the high density snow of $\varepsilon_{sn,bg}$ = 2.4. The measured snow permittivities indicate that the windblown snowcover within the test cells had significantly lower density than that for the high density windpack surrounding the cells. For the underlying sea ice (thickness ~70 cm), we acquired a common midpoint gather (Figure 10) and fit the sea ice/sea water interface reflection with the normal moveout equation. The resulting velocity estimate was v=0.14 m/ns with a corresponding dielectric permittivity of ε_{si} = 4.5. We used these permittivity measurements to forward model the radar response using the reflectivity method described previously. We constructed separate 1D models for the control and test cells using the average oil layer thickness and average snow thickness which varied between the two cells.
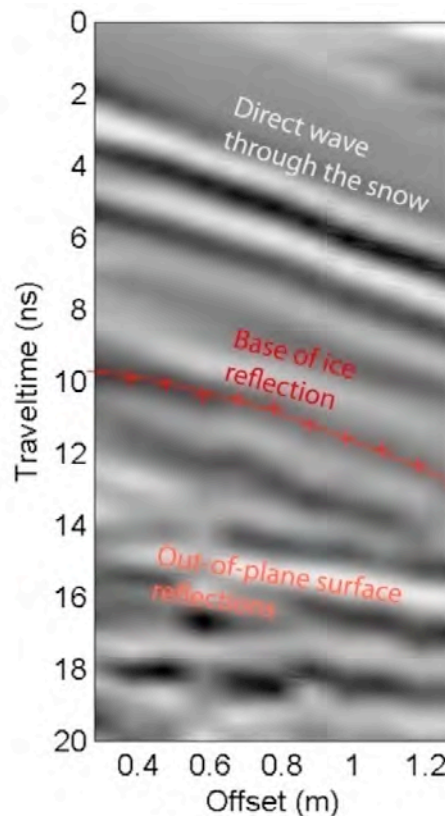

Figure 10. Common midpoint gather acquired over the sea ice. The prominent first arrival is the direct wave through the snow as the shielded antennas emitted very little energy into the air. The traveltime picks for the base of sea ice reflection are shown with red crosses and give an NMO velocity of 0.14 m/ns.

3.3.3   Results

With an oil thickness of 2 cm, the forward model predicted a reduction of 51% in reflection amplitude over the oiled cell relative to the control cell. This response is clearly observed in the field data (Figure 11). After extracting the peak instantaneous amplitude along the snow/sea-ice reflection and averaging over all traces acquired within the cell, we found that the field data at all altitudes and flight speeds show a substantial decrease in reflection strength over the oiled cell (Figure 12). Comparing the clean to contaminated reflection amplitude ratios and averaging over all flight speeds, we found that the field data acquired at a flight altitude of 5 m differ from the model prediction by 16%.   At a flight altitude of 20 m, the difference increases to 29% as the amplitude difference in the field data decreases. This result is expected when we consider that the measured amplitude of the snow/ice reflection is a function of horizontal resolution. The measured amplitude is integrated over the projection of a cone onto the reflecting surface. The cone is defined by the first Fresnel zone which is a function of flight altitude. Far from the source, the radius of the Fresnel zone is given by $\sqrt{\dfrac{\lambda z}{2}}$ where   z is distance to the reflector and λ is the wavelength (Yilmaz, 2001). At 1000 MHz, the diameter of the Fresnel zone at an altitude of 5 m is 1.73 m whereas at 20 m the diameter is 3.46 m.   We expect that our lateral positioning accuracy along the flight line was $\pm$ 2 m relative to the center of the test cell. Therefore, at 20 m the Fresnel zone is approaching the dimensions of our 5 m test cell and the averaged radar amplitude includes a greater contribution of reflectivity that originates outside the test cell.

Model predictions of the change in instantaneous frequency and instantaneous phase at the peak of the envelope function were 10 MHz and 33° respectively. The corresponding measured values for the field test were -3 $\pm$100 MHz and 35° $\pm$ 50°. The predicted change in instantaneous frequency for this spill scenario is just 0.8% of the dominant frequency. Other spill scenarios can produce a large instantaneous frequency anomaly but this is entirely case dependent. The mean instantaneous phase difference in the field data was remarkably close to the predicted change, however the large standard deviation indicates the high sensitivity of this measurement to noise.

In a second modeling run, we predicted the response for 2 cm of oil, but replaced the low density snow permittivity with that for the high density, windpacked snow.   The relative amplitude change is similar to that for the windblown snow (Figure 12) indicating that for a broad range of snow densities we would expect a similar amplitude anomaly.

A

B
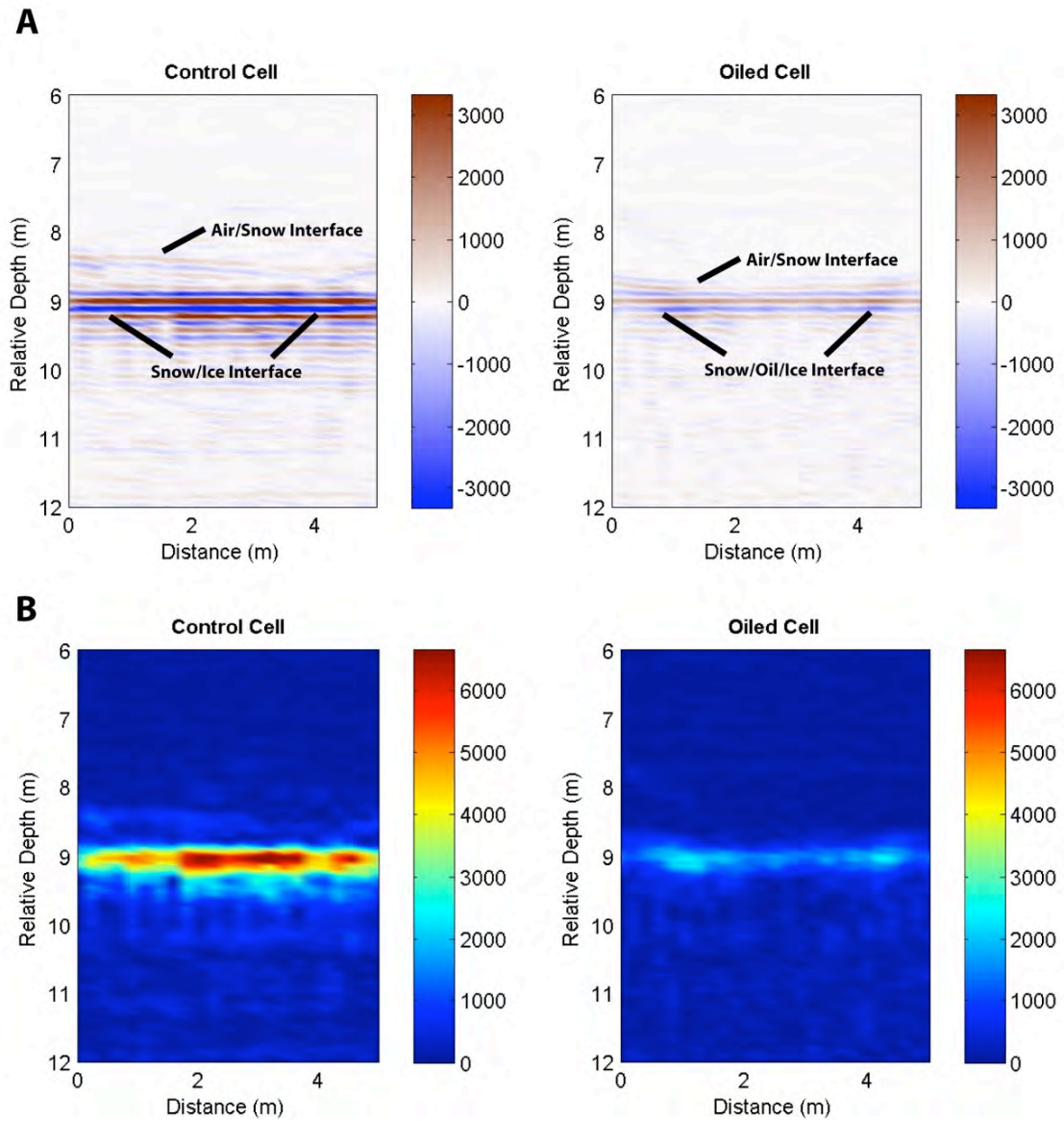
Figure 11. A) Plot of recorded GPR data acquired over the control and oiled cells at an altitude of 5m and speed of 2.57 m/s. B) Plot of reflection strength for the data shown in A. All data are plotted with the same amplitude scaling. Where the oil film is present, the reflection strength is reduced by ~ 45% as predicted by numerical modeling.
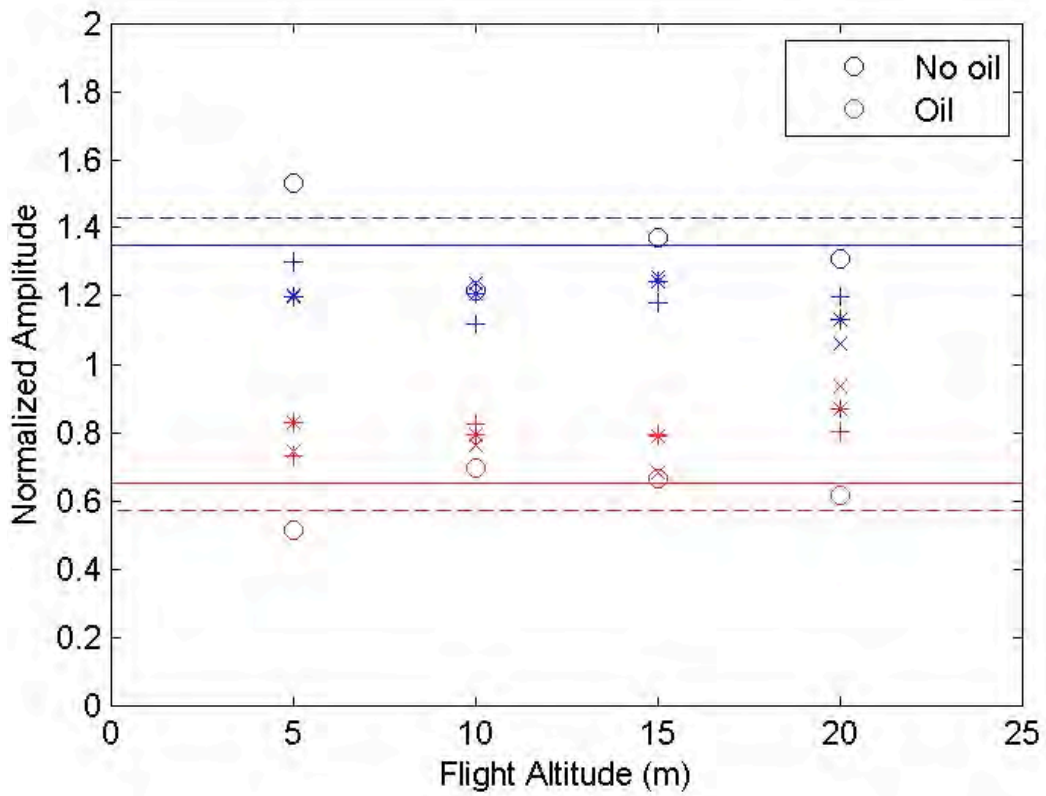
Figure 12. Summary of airborne radar results at speeds of 2.57 m/s (o), 5.14 m/s (+), 7.71 m/s(*), and 10.3 m/s (x). Solid and dashed lines show the predicted amplitudes using the wind blown (low density) and undisturbed snow (high density) properties respectively. Amplitudes are normalized to the average of the clean and contaminated reflections. In all cases the amplitude of the snow-ice interface in the oiled cell is significantly lower than that in the control cell.

4   DISCUSSION

4.1 Oil spill on or within snow

An obvious question is whether the complex reflectivity pattern we observed in our model of oil located on and within snow (Figure 5) would be discerned from the typical background response. This question is particularly apt since the amplitude of reflections from the oil boundaries is comparable to what might be observed due to density contrasts that naturally occur in snow. Typical snow stratigraphy occurs in regular eolian depositional patterns. As the oil migrates through the snow, reflections from these depositional interfaces would be disturbed by the complex pattern of scattering resulting from the irregular distribution of oil and this would produce a signature significantly different from the natural background response.

In dry snow, we expect that oiled zones should be differentiable by an experienced interpreter. Ice layers complicate the interpretation as these high amplitude reflectors tend to be discontinuous and will naturally produce a variable reflection response. Further, the presence of ice layers necessarily requires that liquid water has been present in the snow. Water will flow under gravitational forces along paths similar to the oil and may generate similar reflection patterns, but with higher amplitude. Locating oiled zones, will therefore be most difficult in snow that has undergone melt, or has been disturbed by human activity. In these and all cases however, radar will provide additional information and may help identify likely locations of contaminated snow that may speed remediation activities.

4.2 Oil spill at the base of the snow

The large decrease in reflection amplitude that occurs when oil present at the interface between snow and ice or frozen soil at the base of the snowpack suggests that amplitude analysis alone may be a robust indicator of oil. When the oil is present in thick pools, as in the Prudhoe Bay spill simulation, the oil contaminated layer is well resolved and a high resolution map of oil thickness may be produced through acquisition and interpretation of a 3D GPR survey conducted from an airborne platform. A 3D GPR survey would provide higher density lateral sampling of the oiled zone than manual probing and thereby has the potential to improve the volume estimate. Additionally, by minimizing the need for the manual probe survey the safety of characterization operations would be improved.

A large decrease in amplitude is also predicted for sub-resolution layers of oil at the base of the snow. In this case the amplitude is a function of both the interfering reflections from the top and bottom of the oil layer as well as the decrease in impedance contrast at the ice boundary. The agreement between the synthetic data and our field data from Svalbard is remarkable; we assert that this degree of quantitative agreement with model data is rarely observed in field data. This may be somewhat surprising given the heterogeneity of snow thickness over the test cells which varied both within the cells and between the cells. However, our 1D modeling results indicate that while the amplitude anomaly depends on the density of the overlying snow, the variation in snow thickness causes only minor amplitude changes (Figure 4). Our field results are consistent with these modeling observations. The ~50% reduction in amplitude observed for just a 2 cm thick layer of oil is easily observed in the field data and is well above the noise level. This is an exciting result, and suggests that amplitude analysis alone may be a rapid indicator of oil present at the interface between snow and the underlying ice or frozen soil, allowing spill responders to conduct near real-time evaluation in the field.

Instantaneous phase and frequency measurements from our field test data closely agreed with model predictions. However the high degree of variability in both of these measurements indicates high sensitivity to noise and suggests that these measurements may not be adequately robust for this application. Despite this potential problem, the attributes are easily computed once the data have been acquired and may provide supplemental information that is useful when used in conjunction with the amplitude information.

One factor not addressed in this study, but that could enhance the detection of oil under snow on sea ice is the natural tendency for a layer of brine to accumulate at the snow/ice interface. On natural sea ice, brine will be wicked into the lower levels of the snow pack resulting in an increase in electrical conductivity and permittivity close to the snow/ice interface. If oil is present at this interface, it will block this wicking action, thereby enhancing the anomaly related to the change in electric properties. In that case, our modeled response can be considered conservative compared to the anomaly that would likely be observed for actual field spills onto thin ice before the winter snow cover has had a chance to accumulate.

5 CONCLUSIONS

Our numerical and field results indicate that readily available, commercial GPR systems can be used effectively to detect crude oil spills within or under snow in the Arctic environment. Simple observations of reflection amplitude appear to be a robust indicator of the presence of oil trapped at the snow/ice interface, and a measurable response may be observed at oil thicknesses as small as 1 cm. Further, with measurement of the electric properties of the snow, oil, and underlying medium at a given field site, it is possible to quantitatively predict the GPR response or conversely to potentially estimate spill thickness based on the recorded GPR response. Oil contained within the snowpack may be more difficult to differentiate from the uncontaminated snow, particularly in a complicated snowpack such as a ripe spring snow that contains meltwater and ice layers. In all cases, spill responders must recognize that the GPR interpretations cannot provide absolute information about the location of a spill but may be used as a guide to improve the efficiency of characterization operations.

A recommended working model for spill responders is to first acquire measurements of the electrical properties of the snow, oil, and ice in the vicinity of the spill. These data can be acquired rapidly using the methods described in this study. With this information, the expected radar response can be predicted using available modeling tools thereby increasing the efficiency and accuracy with which field data can be interpreted.

This is the first detailed assessment of the potential for GPR to detect oil spills in and under snow. Further field work is necessary to fully assess GPR capability, however our results show that GPR surveying is a tool that can add substantial value to spill characterization and should be integrated into spill response plans in snow covered regions. Our conclusions come with the caveat that GPR will not produce a unique indicator of oil. Rather, oil identification is a study of anomalies and the spill will be located only if the GPR data in the contaminated areas and the undisturbed snow differ sufficiently that a trained interpreter can identify a significant change in the responses. Of course this working model has a long history of successful application in the detection of hydrocarbon reservoirs from seismic reflection data. The same approach can be applied to GPR reflection data in the near-surface to locate and characterize oil spills. Work has commenced on a new project to develop a more powerful Frequency Modulated Continous Wave (FMCW) radar that will expand the window of opportunity for detecting oil trapped under or within an ice sheet from a low-flying helicopter (DF Dickins and Boise State Univ. – 2010 in progress).

6 REFERENCES AND BIBLIOGRAPHY

Arcone, S.A., E.F. Chacho, Jr., and A.J. Delaney, 1992, Short-pulse radar detection of groundwater in the Sagavanirktok River Floodplain in early spring: Water Resources Research, **28**, 2925-2936.

Arcone, S.A., D.E. Lawson, A.J. Delaney, J.C. Strasser, and J.D. Strasser, 1998, Ground-penetrating radar reflection profiling of groundwater and bedrock in an area of discontinuous permafrost: Geophysics, **63**, 1573-1584.

Best, H., J.P. McNamara, and L. Liberty, 2005, Association of ice and river channel morphology using ground-penetrating radar in the Kuparuk River, Alaska: Arctic, Antarctic, and Alpine Research, **37**, 157-162.

Bradford, J.H., 2007, Frequency dependent attenuation analysis of ground-penetrating radar data: Geophysics, **72**, J7-J16.

Bradford, J.H., and J.C. Deeds, 2006, Ground-penetrating radar theory and application of thinbed offset dependent reflectivity: Geophysics, **71**, K47-K57.

Bradford, J.H., D.F. Dickins, and L. Liberty, 2008, Locating oil spills under sea ice using ground-penetrating radar: The Leading Edge, **27**, 1424-1435.

Bradford, J.H., J.T. Harper, and J. Brown, 2009, Complex dielectric permittivity measurements from ground-penetrating radar data to estimate snow liquid water content in the pendular regime: Water Resources Research, **45**, W08403.

Bradford, J.H., and Y. Wu, 2007, Instantaneous spectral analysis: Time-frequency mapping via wavelet matching with application to 3D GPR contaminated site characterization: The Leading Edge, **26**, 1018-1023.

Butt, K., P. O'Reilly, and E. Reimer, 1981, A field evaluation of impulse radar for detecting oil in and under sea ice, C-CORE, St. John's, 1981, APOA Contract Report 169, Calgary, AB.

Chopra, S., and K.J. Marfurt, 2005, Seismic attributes - A historical perspective: Geophysics, **70**, 3SO-28SO.

Christensen, K.E., 2008, Observations of fuel transport on sea ice from two fuel release events, with relevance to site assessment and closure: Cold Regions Science and Technology, **53**, 92-101.

Daniels, D.J., 2007, Ground penetrating radar, The Institution of Engineering and Technology.

Delaney, A.J., S.A. Arcone, and E.F. Chacho, Jr., 1990, Winter short-pulse radar studies on the Tanana River, Alaska: Arctic, **43**, 244-250.

DF Dickins Associates and Boise State University, 2010. Detecting oil on and under sea ice using ground penetrating radar: Development of a new airborne system. JIP funded by ACS, ExxonMobil, MMS, Shell Oil, and Statoil (in progress).

Fingas, M., and C. Brown, 2000, A review of the status of advanced technologies for the detection of oil in and with ice: Spill science and technology, **6**, 295-302.

Goodman, R., 2008, Oil under ice detection: What is the state-of-the-art?, *in* Davidson, W.F., Lee, K., and Cogswell, A., Eds., Oil spill response: A global perspective: Springer Science + Business Media B.V.

Goodman, R., H. Jones, and M. Fingas, 1985a, The detection of oil under ice using acoustics: Conference on port and ocean engineering under Arctic conditions, Danish Hydraulic Institute, 903-916.

Goodman, R.H., A.M. Dean, and M.F. Fingas, 1985b, The detection of oil under ice using electromagnetic radiation: Conference on port and ocean engineering under Arctic conditions, Danish Hydraulic Institute, 895-902.

Greaves, R.J., D.P. Lesmes, J.M. Lee, and M.N. Toksoz, 1996, Velocity variation and water content estimated from multi-offset, ground-penetrating radar: Geophysics, **61**, 683-695.

Harper, J.T., and J.H. Bradford, 2003, Snow stratigraphy over a uniform depositional surface: Spatial variability and measurement tools: Cold Regions Science and Technology, **37**, 289-298.

Huisman, J.A., S.S. Hubbard, J.D. Redman, and A.P. Annan, 2003, Measuring soil water content with ground-penetrating radar: A review: Vadose Zone Journal, **2**, 476-491.

Jones, H.W., and H.W. Kwan, 1982, The detection of oil spills under Arctic ice by ultrasound: 5th Annual Arctic Marine Oil Spill Technical Seminar, Environemental Protection Service, 391-411.

Kovacs, A., 1977, Sea ice thickness profiling and under-ice oil entrapment: 9th Annual offshore technology conference, 547-554.

Kovacs, A., and R.M. Morey, 1978, Radar anistotropy of sea ice due to preferred azimuthal orientation of the horizontal c aces of ice crystals: Journal of Geophysical Research, **83**, 6037-6046.

Kovacs, A., and R.M. Morey, 1992, Estimating sea ice thickness from impulse radar sounding of flight time data, Geological Survey of Canada Report #90-04, 117-124.

Langham, E.J., 1981, Physics and properties of snowcover, *in* Gray, D.M., and Male, E.M., Eds., Handbook of snow: The Blackburn Press, 275-337.

Levander, A.R., 1989, Finite-difference forward modeling in seismology, *in* James, D.E., Ed., Encyclopedia of solid earth geophysics: Van Nostrand Rheinhold.

Lewis, E.O., C.E. Livingstone, C. Garrity, and J.R. Rossiter, 1994, Properties of snow and ice, *in* Haykin, S., Lewis, E.O., Raney, R.K., and Rossiter, J.R., Eds., Remote sensing of sea ice and icebergs: John Wiley & Sons, Inc., 21-96.

Løseth, L.O., and B. Ursin, 2007, Electromagnetic fields in planarly layered anisotropic media: Geophysical Journal International, **170**, 44-80.

Lundberg, A., H. Thunehed, and J. Bergstrom, 2000, Impuse radar snow surveys - influence of snow density: Nordic Hydrology, **31**, 1-14.

Mackay, D., 1974, Absorption and flow of oil into snow, *in* Mackay, D., Charles, M.E., and Phillips, C.R., Eds., The Physical Aspects of Crude Oil Spills on Northern Terrain: Department of Indian and Northern Affairs, Task Force on Northern Development Report No. 73-42, 98-151.

Mackay, D., P. Leinonen, J. Overall, and B. Wood, 1975, The behavior of oil spilled on snow: Arctic, **28**, 9-20.

Marshall, H.P., and G. Koh, 2008, FMCW radars for snow research: Cold Regions Science and Technology, **47**, 108-117.

Marshall, H.P., M. Schneebeli, and G. Koh, 2007, Snow stratigraphy measurements with high-frequency radar: comparison with snow micro-penetrometer: Cold Regions Science and Technology, **47**, 108-117.

McMinn, T.J., 1972, Crude oil behavior on Arctic winter ice: Final Report, Office of Research and Development, United States Coast Guard, Project 734108, NTIS Publication No. AP-754.

Morey, R.M., A. Kovacs, and G.F.N. Cox, 1984, Electromagnetic properties of sea ice: Cold Regions Science and Technology, **9**, 53-75.

Müller, G., 1985, The reflectivity method: A tutorial: Journal of Geophysics, **58**, 153-174.

Nyland, D., 2004, Profiles of floating ice in Arctic regions using GPR: The Leading Edge, **23,** No., 7, 665-668.

Orlando, L., 2002, Detection and analysis of LNAPL using the instantaneous amplitude and frequency of ground-penetrating radar data: Geophysical Prospecting, **50**, 27-41.

Owens, E.H., D.F. Dickins, and G.A. Sergy, 2005, The behavior and documentation of oil spilled on snow- and ice-covered shorelines: Interntional Oil Spill Conference.

Ritter, D.F., R.C. Kochel, and J.R. Miller, 2002, Process Geomorphology, Waveland Press.

Sand, K., and O. Bruland, 1998, Application of georadar for snow cover surveying: Nordic Hydrology, **29**, 361-370.

Schwamborn, G.J., J.K. Dix, J.M. Bull, and V. Rachold, 2002, High-resolution seismic and ground penetrating radar - Geophysical profiling of a thermokarst lake in the Western Lena Delta, Northern Siberia: Permafrost and Periglacial Processes, **13**, 259-269.

Speight, J.G., 2003, Perry's standard tables and formulas for chemical engineers, McGraw-Hill.

Wharton, R.P., G.A. Hazen, R.N. Rau, and D.L. Best, 1980, Electromagnetic propagation logging: advances in technique and interpretation: 55th Annual Fall Technical Conference and Exhibition, Society of Petroleum Engineers. Paper 9267.

Widess, M.B., 1973, How thin is a thin bed?: Geophysics, **38**, 1176-1180.

Yilmaz, O., 2001, Seismic data analysis, Society of Exploration Geophysicists.